Distribution of Electrical Potential, pH, Free Ca^{2+}, and Volume Inside Cultured Adult Rabbit Cardiac Myocytes During Chemical Hypoxia: A Multiparameter Digitized Confocal Microscopic Study

Enrique Chacon, Jeffrey M. Reece, Anna-Liisa Nieminen, George Zahrebelski, Brian Herman, and John J. Lemasters

Laboratories for Cell Biology, Department of Cell Biology & Anatomy and Curriculum in Toxicology, University of North Carolina at Chapel Hill, Chapel Hill, North Carolina 27599 USA

ABSTRACT Exploiting the optical sectioning capabilities of laser scanning confocal microscopy and using parameter-specific fluorescent probes, we determined the distribution of pH, free Ca^{2+}, electrical potential, and volume inside cultured adult rabbit cardiac myocytes during ATP depletion and reductive stress with cyanide and 2-deoxyglucose ("chemical hypoxia"). During normoxic incubations, myocytes exhibited a cytosolic pH of 7.1 and a mitochondrial pH of 8.0 (ΔpH = 0.9 units). Sarcolemmal membrane potential ($\Delta\Psi$) was −80 mV, and mitochondrial $\Delta\Psi$ was as high as −100 mV, yielding a mitochondrial protonmotive force (Δp) of −155 mV ($\Delta P = \Delta\Psi - 60\Delta$pH). After 30 min of chemical hypoxia, mitochondrial ΔpH decreased to 0.5 pH units, but mitochondrial $\Delta\Psi$ remained essentially unchanged. By 40 min, ΔpH was collapsed, and mitochondrial and cytosolic free Ca^{2+} began to increase. Mitochondrial and sarcolemmal $\Delta\Psi$ remained high. As Ca^{2+} rose, myocytes shortened, hypercontracted, and blebbed with a 30% decrease of cell volume. After hypercontraction, extensive mitochondrial Ca^{2+} loading occurred. After another few minutes, mitochondria depolarized completely and released their load of Ca^{2+}. After many more minutes, the sarcolemmal permeability barrier broke down, and viability was lost. These studies demonstrate a sequence of subcellular ionic and electrical changes that may underlie the progression to irreversible hypoxic injury.

INTRODUCTION

ATP is the immediate energy source for most biological energy-requiring reactions. In aerobic tissues like heart, the bulk of ATP is formed by mitochondria. During mitochondrial respiration, free energy is liberated to drive ATP synthesis at three coupling sites: Sites 1, 2, and 3. According to Mitchell's chemiosmotic hypothesis, each of the three coupling sites pumps protons outwards across the mitochondrial inner membrane, generating an electrochemical gradient of protons ($\Delta\mu_{H^+}$), or equivalently, a protonmotive force ($\Delta p = \Delta\mu_{H^+}/F$) (Mitchell, 1966). In addition to driving ATP synthesis, Δp supports other energy requiring reactions in mitochondria, such as ion transport and transhydrogenation. Hence, maintenance of Δp is crucial for the survival of aerobic cells.

Δp is comprised of two components, a membrane potential ($\Delta\Psi$) and a pH gradient (ΔpH)

$$\Delta p = \Delta\Psi - 2.3RT\Delta\text{pH} \quad (1)$$

where R is the ideal gas constant, T is absolute temperature, and Δp has units of mV. At physiological temperatures, Eq. 1 reduces to

$$\Delta p = \Delta\Psi - 60\Delta\text{pH}. \quad (2)$$

Previously, techniques have been developed to measure average $\Delta\Psi$ and ΔpH of mitochondria in cell suspensions and cell cultures (Hoek et al., 1980). However, the magnitude of $\Delta\Psi$ and pH of individual mitochondria in single cells has been much more difficult to assess. Mitochondria are too small to measure $\Delta\Psi$ and pH reliably using electrodes. Consequently, mitochondrial $\Delta\Psi$ is usually measured from the equilibrium distribution of membrane-permeant cations (Hoek et al., 1980; Nicholls, 1974; Rottenberg, 1975). Recently, using laser scanning confocal microscopy, Farkas and co-workers showed that confocal microscopy can measure $\Delta\Psi$ in mitochondria of living cells (Farkas et al., 1989). Here, we extend this approach to image electrical potential, pH, free Ca^{2+}, and cell topography of living cardiac myocytes in culture under conditions simulating hypoxic injury. We show that a distinctive progression of subcellular electrical and ionic changes precedes the onset of irreversible cell death.

MATERIALS AND METHODS

Isolation and culture of adult rabbit cardiac myocytes

Adult rabbit cardiac myocytes were isolated by enzymatic digestion by modification of the procedure of Haddad et al. (1988) as described in detail

Received for publication 8 April 1993 and in final form 10 November 1993.

Address reprint requests to Dr. John J. Lemasters, Department of Cell Biology & Anatomy, The University of North Carolina at Chapel Hill, CB# 7090, 236 Taylor Hall, Chapel Hill, NC 27599. Tel.: 919-966-5507; Fax: 919-966-1856.

This work was supported, in part, by Grants HL48769, AG07218, and DK37034 from the National Institutes of Health and Grant N00014–89-J-1433 from the Office of Naval Research. E. Chacon is the recipient of a National Research Service Award through Grant T32ES07126 to the Curriculum in Toxicology from the National Institute of Environmental Health Sciences. A preliminary report of portions of this work was presented at the Sixth International Congress of Toxicology, Rome, 25 June–3 July 1992 (Chacon et al., 1992*b*).

Dr. Chacon's present address is Cedra Corporation, 8609 Cross Park, Austin, TX 78754.

Abbreviations used: AM, acetoxymethyl ester; ATP, adenosine triphosphate; CAT, computerized axial tomography; HEPES, N-(2-hydroxyethyl)-piperazine-N'-2-ethanesulfonic acid; KRH, Krebs-Ringer HEPES buffer; TMRM, tetramethylrhodamine methylester.

0006-3495/94/04/942/11 $2.00

elsewhere (Chacon et al., 1993a). Briefly, white New Zealand rabbits weighing 3–4 kg were heparinized by administration of 250 units of sodium heparin/kg of body weight via a 22-gauge butterfly catheter placed in the marginal ear vein. Surital (150 mg) was administered by the same route for anesthesia. The chest cavity was opened and immediately irrigated with ice-cold Ca^{2+}-free Buffer A (5 mM KCl, 110 mM NaCl, 1.2 mM NaH_2PO_4, 28 mM $NaHCO_3$, 30 mM glucose, 20 mM butanedione monoxime, 0.05 units/ml insulin, 250 μM adenosine, 1 mM creatine, 1 mM carnitine, 1 mM octanoic acid, 1 mM taurine, 10 units/ml penicillin, 10 μg/ml streptomycin, and 25 mM HEPES, pH 7.30).

Each heart was mounted on a modified Langendorf perfusion apparatus and perfused at a rate of 25 ml/min with Buffer A saturated with 95% O_2, 5% CO_2 in a retrograde fashion at 37°C from a height of 100 cm. After 5 min, a digestion buffer consisting of Buffer A containing 25 μM $CaCl_2$, 68 units/ml collagenase type 2, and 70 units/ml hyaluronidase type 1-S was recirculated for 20 min. Using scissors, the ventricles were excised below the atrioventricular junction, and four incisions towards the apex were made. Using sterile forceps, the tissue was then gently agitated in Buffer A supplemented with 25 μM $CaCl_2$ and 0.5 mg/ml trypsin 1:250 for 30 min to release the rod-shaped myocytes.

The cell suspension was placed in 50 ml of polypropylene tubes and centrifuged at 20 × g for 2 min. The supernatant was discarded, and the pellet was resuspended in Buffer B (Joklik's medium and medium 199 (1:1 mixture) supplemented with 20 mM butanedione monoxime, 1 mM creatine, 1 mM taurine, 1 mM octanoic acid, 1 mM carnitine, 0.05 units/ml insulin, 10 units/ml penicillin, and 10 μg/ml streptomycin). After 10 min, the suspended cells were pelleted at 20 × g for 2 min. The supernatant was discarded and the pellet was resuspended in Buffer C (Buffer B supplemented with 0.5 mg/ml trypsin 1:250, but without butanedione monoxime). After 30 min, the cell suspension was centrifuged at 20 × g for 2 min. The supernatant was again discarded, and the pellet was resuspended in 15 ml of nutrient medium (Buffer B without trypsin and butanedione monoxime). Cells were counted and plated at a density of 15,000/cm^2 on glass coverslips coated with laminin (10 μg/cm^2). Experiments were conducted 1 day after the initial plating of the myocytes.

Fluorescence microscopy

Fluorescence images were collected with a Bio-Rad MRC-600 laser scanning confocal microscope mounted on a Nikon Diaphot inverted microscope. The objective lens was a Nikon 60X N.A. 1.4 planapochromat or a 40X N.A. 1.3 fluor lens. A pinhole setting of 3 was used to maximize optical sectioning. Confocal optical sections were 0.8–0.9 μm in thickness (Lemasters et al., 1993). Lateral resolution was diffraction-limited, i.e., about 0.2 μm. The 488- and 568-nm lines of an argon-krypton laser were directed to the sample by a double dichroic mirror. Excitation light was attenuated with a 1% neutral density filter to minimize photobleaching and photodamage. Fluorescence of TMRM excited at 568 nm was collected through a 595-nm-long pass barrier filter. Fluorescence of Fluo-3 excited at 488 nm was collected through a 522 nm (35 nm band pass) barrier filter. Fluorescence of SNARF-1 excited at 568 nm was directed to separate photomultipliers using 585 (10 nm band pass)- and 620-nm-long pass barrier filters and a 595-nm-long pass dichroic reflector. The ratio of SNARF-1 fluorescence at >620 nm to that at 585 nm was used to estimate the intracellular pH as described below. Fluorescence of calcein excited at 488 nm was collected through a 510 nm dichroic reflector and a 515-nm-long pass barrier filter. A more complete description of the confocal imaging system used may be found in Lemasters et al. (1993).

Determination of electrical potential

Electrical potentials were estimated from the distribution of TMRM, a membrane-permeant cationic fluorophore (Ehrenberg et al., 1988). To load TMRM, cultured myocytes were incubated with 600 nM TMRM in culture medium for 20 min at 37°C. The cells were then placed on the microscope stage in KRH buffer (110 mM NaCl, 5 mM KCl, 1.25 mM $CaCl_2$, 1.0 mM Mg_2SO_4, 0.5 mM Na_2HPO_4, 0.5 mM KH_2PO_4, 20 mM HEPES, pH 7.4) containing 150 nM TMRM to maintain equilibrium distribution of the fluorophore. Experiments were then initiated after another 15 min of incubation. In control experiments, TMRM labeling was stable for more than an hour.

The Bio-Rad MRC-600 laser scanning confocal unit was equipped with a nonlinear log amplifier called an enhance control. An enhance control setting of +4 was used for measurement of TMRM fluorescence. Output voltage of the enhance circuit is given by

$$V_\gamma = 1 + A \ln(V_{PMT} + e^{-1/A}) \quad (3)$$

where V_γ is output voltage of the enhance circuit, V_{PMT} is input voltage to the enhance circuit from the photomultiplier, and A is 0.206. Thus, V_γ is 0 volts (0 pixel intensity) when V_{PMT} is 0 volts, and 1 volt (255 pixel intensity) when V_{PMT} is 0.99 volts. At voltages in between 0 and 0.99 volts, V_γ is an exponential function of V_{PMT}. Eq. 3 can be solved for V_{PMT}

$$V_{PMT} = e^{(V_\gamma - 1)/A} - e^{-1/A}. \quad (4)$$

TMRM distributes into negatively charged cellular compartments in accordance with the Nernst equation

$$\Delta\Psi = -60 \log(F_{in}/F_{out}) \quad (5)$$

where F_{in} and F_{out} are TMRM concentrations inside and outside the compartment of interest. TMRM concentration is proportional to fluorescence, which in turn is proportional to V_{PMT}.

To establish the appropriate imaging conditions for membrane potential quantitation, black level (dark current) of the Bio-Rad MRC-600 was set to zero while focusing within the coverslip below the cell. This avoids the necessity of a background subtraction, which is not easily performed with the enhance circuit. A full-field image histogram of the black level was performed to ensure that 50% of the pixels exhibited a zero intensity value corresponding to a $V_{PMT} \leq 0$. After adjustment of the black level, a focal plane within the specimen was chosen, and an image was collected. V_{PMT} corresponding to intensity outside the cell was then determined, using an area histogram and application of Eq. 4. From V_{PMT} outside the cell ($V_{PMT(out)}$), the electrical potential anywhere inside the cell relative to outside was calculated

$$\Delta\Psi = -60 \log(V_{PMT(in)}/V_{PMT(out)}) \quad (6)$$

where $V_{PMT(in)}$ is V_{PMT} for any pixel inside the cell as calculated from Eq. 4.

To display the distribution of electrical potentials inside cells relative to outside, pseudocolor look-up tables were created to convert pixel values of 0 to 255 (corresponding to V_γ of 0 to 1 volt) to $\Delta\Psi$. Table 1 illustrates computed $\Delta\Psi$ values for different pixel intensities when extracellular V_γ was 2.0 pixel units (0.0078 volts). Different look-up tables were required for each value of $V_{PMT(out)}$, and a program was written in BASIC to construct these pseudocolor look-up tables in a format compatible with Bio-Rad's SOM and COMOS confocal software.[1]

Measurements of intracellular pH

Intracellular pH was estimated with SNARF-1, a pH-sensitive fluorophore with a pK_a of about 7.5 (Bassnett et al., 1990; Sesek et al., 1991). Excited at 488 nm (an argon laser line), SNARF-1 fluorescence at 585 nm decreased with increasing pH, whereas fluorescence at 640 nm increased (Fig. 1 *A*). The isoemissive point was about 610 nm. When SNARF-1 was excited at the 568 nm (one of the argon-krypton laser lines), fluorescence at 640 nm increased as pH increased, and 585 nm was the isoemissive point (Fig. 1 *B*). At pH 7.5, the intensity of fluorescence excited at 568 nm was greater than that at 488 nm excitation (Fig. 1 *C*) because 568 nm is an absorbance maximum of the dye. Hence, for confocal imaging, we used the 568-nm line of the argon-krypton laser for excitation and collected confocal fluorescence images at emission wavelengths of >620 nm and 585 ± 5 nm. The ratio of fluorescence emitted at these two different wavelengths was then used to estimate pH.

Cultured myocytes were loaded with 5 μM SNARF-1 acetoxymethyl ester for 45 min in culture medium at 37°C. The cells were washed twice

[1] This program is available upon request.

TABLE 1 Calculation of electrical potentials from pixel values obtained using an enhance circuit

Pixel Value	V_γ	V_{PMT}	ψ	Pixel Value	V_γ	V_{PMT}	ψ
	V	*V*	*mV*		*V*	*V*	*mV*
10	0.039	0.002	−44	140	0.549	0.104	−152
20	0.078	0.004	−65	150	0.588	0.128	−158
30	0.118	0.006	−78	160	0.627	0.156	−163
40	0.157	0.009	−88	170	0.667	0.190	−168
50	0.196	0.012	−97	180	0.706	0.232	−173
60	0.235	0.017	−104	190	0.745	0.282	−178
70	0.275	0.022	−111	200	0.784	0.343	−183
80	0.314	0.028	−118	210	0.824	0.417	−188
90	0.353	0.035	−124	220	0.863	0.506	−193
100	0.392	0.045	−130	230	0.902	0.614	−198
110	0.431	0.055	−136	240	0.941	0.744	−203
120	0.471	0.069	−141	250	0.980	0.901	−208
130	0.510	0.085	−147	255	1.000	0.992	−211

Calculations of electrical potential (ψ) were made using Eqs. 4 and 6 assuming an enhance setting of 4 (A = 0.206) and an extracellular V_γ of 0.00784 volts. V_{PMT} is photomultiplier voltage. V_γ equals the pixel value divided by 255.

and placed on the microscope stage in KRH. Using 568-nm excitation, fluorescence emitted at 585 nm and >620 nm was imaged simultaneously using two detectors. After background subtraction, the images were divided into one another on a pixel-by-pixel basis. The resulting ratios were converted to pH values based on an in situ pH calibration of SNARF-1. For in situ calibration, SNARF-1-loaded myocytes were incubated with 10 μM nigericin and 5 μM valinomycin in modified KRH buffer, in which NaCl and KCl were replaced by their corresponding gluconate salts to minimize swelling (Kawanishi et al., 1991). Images were then collected as extracellular pH was varied.

Surface topography

To label the intracellular space, myocytes were incubated with 5 μM calcein-AM for 1 h at 37°C in culture medium, washed three times with KRH buffer, and mounted on the microscope stage. Calcein was excited at 488 nm and emitted green fluorescence insensitive to changes of intracellular ions (Haugland, 1992). Serial confocal images of calcein fluorescence were collected as the focal plane was advanced in 1.2-μm increments through cell thickness. Images from 13 focal planes were collected, where each image was a 1.5-s scan. This process was repeated every 15–30 min. Image data sets were transported to a Silicon Graphics Workstation operating VoxelView software (Vital Images, Fairfield, IA) for three-dimensional reconstruction. Reconstructed cells were displayed as solid objects, using contour-dependent shading to emphasize surface topography.

Measurement of intracellular free Ca^{2+}

Intracellular free Ca^{2+} was monitored with the calcium-sensitive fluorophore, Fluo-3 (Minta et al., 1989). Cultured myocytes were loaded with 20 μM Fluo-3 acetoxymethyl ester for 45 min in culture medium at 37°C. Cultures were washed twice and placed on the microscope stage in KRH. The fluorophore was excited using the 488-nm line of the argon-krypton laser.

Chemical hypoxia

To mimic the ATP depletion and reductive stress of hypoxia, myocyte cultures were exposed to 2.5 mM NaCN and 20 mM 2-deoxyglucose in KRH at 37°C, inhibitors of oxidative phosphorylation and glycolysis, respectively. Previous experiments in hepatocytes and neonatal myocytes have shown that such treatment causes rapid ATP depletion and cell death after about 90 min (Gores et al., 1988; Bond et al., 1991). Calcein, SNARF-1, and Fluo-3 were well retained until the onset of cell death, at which point

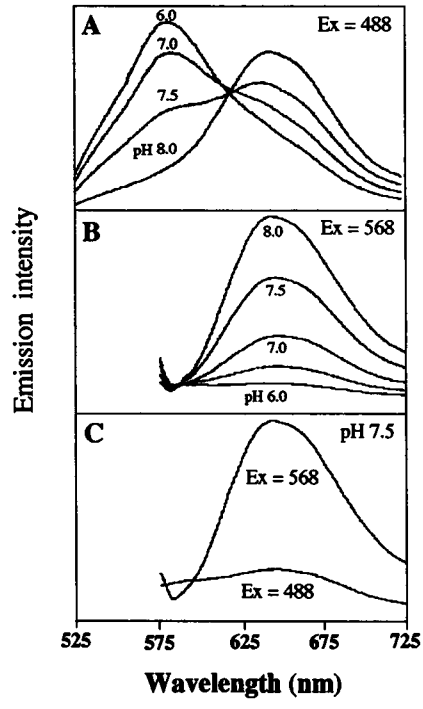

FIGURE 1 Fluorescence emission spectra of SNARF-1. Fluorescence emission spectra were acquired for SNARF-1 (6 μM) in KRH buffer at different pH. In *A*, SNARF-1 was excited at 488 nm. In *B*, SNARF-1 was excited at 568 nm. In *C*, emission spectra were acquired at pH 7.5 at excitation wavelengths of 568 nm (*upper trace*) and 488 nm (*lower trace*). Spectra were acquired from a 1-cm cuvette in a Perkin-Elmer Model 850–40 fluorescence spectrophotometer (Norwalk, CT) using 0.5-nm slits.

the fluorophores were released rapidly (Lemasters et al., 1993). In control experiments, no leakage was apparent after incubations of an hour or more.

Scanning electron microscopy

Cardiac myocytes on coverslips were fixed with 2% glutaraldehyde in 0.1 M NaPi buffer, pH 7.4, and prepared for observation in a JEOL 820 scanning electron microscope, as described previously (Lemasters et al., 1983).

Reagents

Fluo-3 AM, calcein AM, TMRM, and SNARF-1 AM were purchased from Molecular Probes (Eugene, OR); NaCN, 2-deoxyglucose, trypsin 1:250, and hyaluronidase type 1-S were from Sigma Chemical Co. (St. Louis, MO); collagenase type 2 was from Worthington Biochemical (Freehold, NJ); laminin was from Collaborative Biochemicals (Bedford, MA); and HEPES was from Boehringer Mannheim (Indianapolis, IN).

RESULTS

Scanning electron microscopy

After 1 day in culture, scanning electron microscopy revealed intact myocytes with typical features of adult cells (Fig. 2). Single cellular units were branched rods with beaded rib-like surface structures that represented the impression of subsarcolemmal mitochondria aligned along sarcomeres. At higher power, openings of t-tubules were observed between the beaded ribs (data not shown).

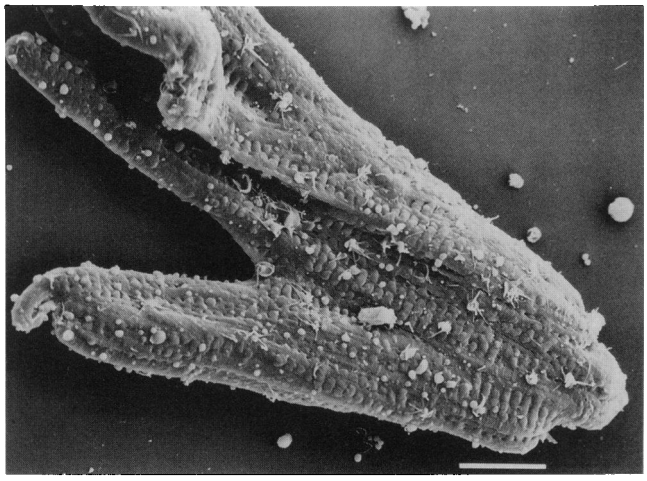

FIGURE 2 Scanning electron microscopy of a cultured adult rabbit cardiac myocyte: a 1-day cultured adult rabbit cardiac myocyte was fixed and prepared for scanning electron microscopy as described in Materials and Methods. Bar is 10 μm.

Three-dimensional reconstruction of calcein-loaded myocytes

Cultured myocytes were loaded with calcein, and confocal images at 1.2 μm increments were collected as the plane of focus was advanced through the thickness of a single myocyte, as described in Materials and Methods. Three-dimensional reconstructions were made to display cell surface topography in a perspective analogous to scanning electron microscopy. Regularly spaced rib-like structures were the dominant surface feature during normoxic incubation (Fig. 3 *A*). Overall, reconstructions of living cells using confocal microscopy closely resembled images obtained from fixed, dehydrated, and metal-coated specimens by scanning electron microscopy (compare with Fig. 2).

To mimic the ATP depletion and reductive stress of anoxia, the myocyte in Fig. 3 *A* was exposed to 2.5 mM NaCN and 20 mM 2-deoxyglucose (chemical hypoxia). After 25 min, no apparent changes of cell surface topography were evident (Fig. 3 *B*). After 40 min of chemical hypoxia, hypercontraction and cell surface blebbing developed (Fig. 3 *C3*). After 90 min, some additional bleb growth was evident, but the overall appearance of the cell was similar to that at 40 min (Fig. 3 *D*). Subsequently, the cell abruptly lost its trapped calcein, indicating breakdown of the sarcolemmal permeability barrier and loss of viability (not shown). Cellular volume was also calculated from the three-dimensional volume reconstructions collected during the progression of cell injury. Initial volume of the myocyte shown in Fig. 3 was 6×10^4 μm^3 (Fig. 4). Volume changed little until the onset of hypercontraction, when cell volume decreased about 30%. Subsequently, little further change of volume was observed.

Distribution of electrical potentials during chemical hypoxia

To measure intracellular electrical potentials, myocytes were loaded with TMRM, and confocal images were collected using an enhance circuit as described in Materials and Methods. Nonconfocal brightfield images were collected simultaneously using a transmitted light detector. Untreated cells showed typical striations in brightfield images (Fig. 5 *A*). Mitochondria were not readily distinguished by brightfield microscopy but were easily observed as spheres and rods in the unprocessed confocal fluorescence image obtained at an enhance circuit setting of 4 (Fig. 5 *B*). In Fig. 5 *C*, the image was pseudocolored to represent electrical potential. Pixel values were converted to V_{PMT} and divided by the average extracellular V_{PMT}. The ratio values were then converted to $\Delta\Psi$ using the Nernst equation (Eq. 6) and displayed using different colors to present a map of electrical potentials within the myocyte.

In areas just under the sarcolemma, in the nucleus, and in a few open spaces between mitochondria, electrical potentials averaging about -80 mV were observed (Fig. 5 *C*). Because electrical potential of the extracellular space was zero, $\Delta\Psi$ was -80 mV across the sarcolemma, which is very close to the expected value. The electrical potential inside mitochondria was in the range of -140 to -180 mV, represented by orange and red in the pseudocolored image (Fig. 5 *C*). Because cytosolic and nuclear potential was -80 mV, the difference, -60 to -100 mV, represents mitochondrial $\Delta\Psi$. However, because not all mitochondria extended fully through the confocal optical slice, higher values most likely represent true mitochondria $\Delta\Psi$ (see Discussion).

The myocyte in Fig. 5 was then exposed to chemical hypoxia. Up to the point of hypercontraction and bleb formation 40 min later, sarcolemmal and mitochondrial $\Delta\Psi$ were essentially unchanged (Fig. 5 *D–F*). Membrane depolarization subsequently occurred after the onset of hypercontraction (see below).

Intracellular pH during chemical hypoxia

Intracellular pH measured by SNARF-1 ratio imaging showed marked heterogeneity in untreated myocytes (Fig. 6 *A*). Subsarcolemmal, intermitochondrial and nuclear areas had a pH in the range of 7.0–7.2, but in regions corresponding to the mitochondria, the maximum pH was about 8.0. Thus, ΔpH across the mitochondrial membrane was as great as 0.9 units. Chemical hypoxia caused a gradual decline of mitochondrial ΔpH. After 30 min of chemical hypoxia, ΔpH decreased to about 0.5 units (Fig. 6 *B*). After 40 min, ΔpH collapsed entirely (Fig. 6 *C*). Closely after collapse of mitochondrial ΔpH, the myocyte hypercontracted and formed surface blebs (Fig. 6 *D*).

Changes of free Ca^{2+} during chemical hypoxia

Cardiac myocytes were also co-loaded with TMRM and Fluo-3. The red fluorescence of TMRM and the green fluorescence of Fluo-3 were imaged simultaneously to measure relative changes of $\Delta\Psi$ and free Ca^{2+}, respectively. In these particular experiments, TMRM fluorescence was imaged without using an enhance circuit. Before chemical hypoxia, the fluorescence images showed

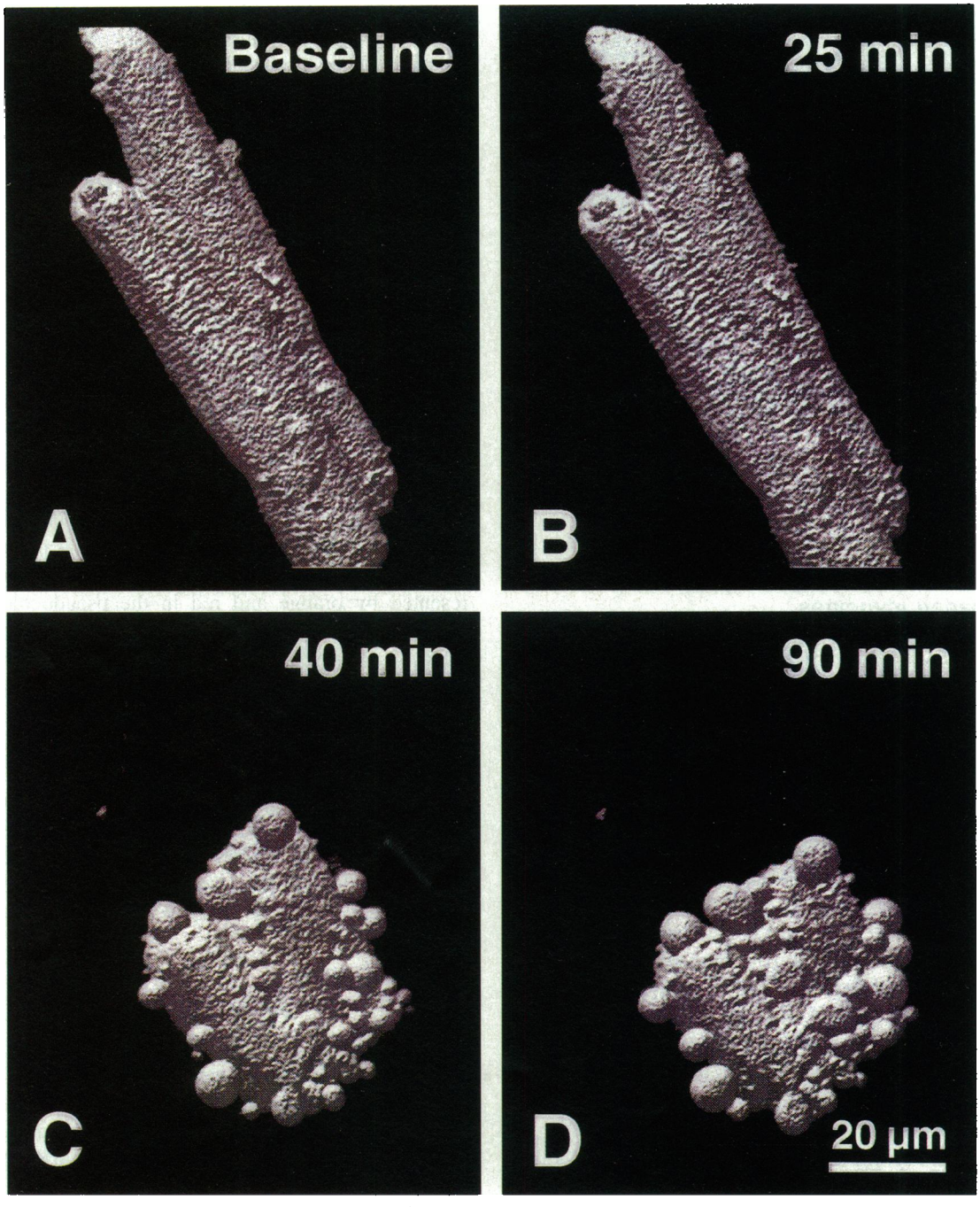

FIGURE 3 Volume renderings of a calcein-loaded cultured cardiac myocyte during chemical hypoxia: a 1-day cultured myocyte was loaded with calcein, and three-dimensional reconstructions of cell shape were generated from confocal fluorescence images as described in Materials and Methods. *A* shows a single myocyte during normoxic incubation (baseline). *B–D* show the myocyte after 25-, 40-, and 90-min exposure to 2.5 mM NaCN and 20 mM 2-deoxyglucose (chemical hypoxia). Note hypercontraction and cell surface blebbing in *C* and *D*.

that mitochondria were polarized and that free Ca^{2+} was low and homogenously distributed within the myocyte (Fig. 7 *A*). After 40 min of chemical hypoxia, free Ca^{2+} began to increase with little or no change of TMRM fluorescence (Fig. 7 *B*). After 50 min, the myocyte began to shorten (Fig. 7 *C*), and after 51 min, it hypercontracted (Fig. 7 *D*). Fluo-3 fluorescence continued to increase during shortening and hypercontraction. Mitochondrial Ca^{2+} loading became especially prominent just at the onset of hypercontraction. Shortly after hypercontraction and mitochondrial Ca^{2+} loading, mitochondria abruptly lost their TMRM fluorescence, indicating depolarization (Fig. 7 *E*). As mitochondria depolarized, their Fluo-3 fluorescence decreased, signifying release of mitochondrial Ca^{2+} (Fig. 7 *E*). Subsequently, Fluo-3 fluorescence decreased to low values (Fig. 7 *F*). This indicated either loss of fluorophore or return of free Ca^{2+} to levels near baseline. The latter may be more likely, because myocytes retained calcein for more than 45 min after the onset of hypercontraction (Fig. 3).

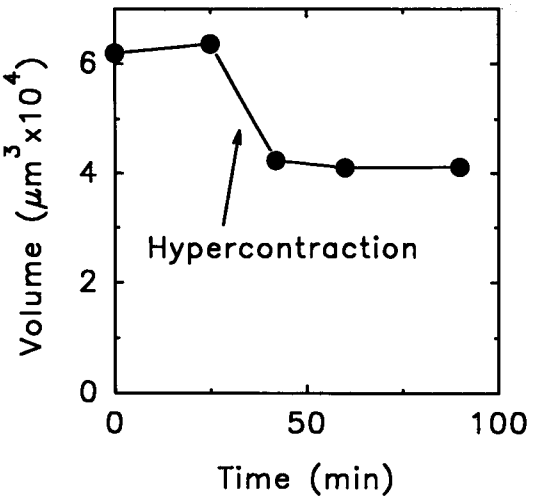

FIGURE 4 Volume of a single cardiac myocyte during chemical hypoxia: the volume of the myocyte shown in Fig. 3 is plotted against time of chemical hypoxia. The arrow marks the onset of hypercontraction.

DISCUSSION

Shape and volume changes during chemical hypoxia

Confocal microscopy creates images with depths of field of less than 1 μm. In essence, a confocal microscope acts as a CAT scanner for cells. The improved resolving power of confocal microscopy over conventional microscopy is analogous to that for CAT scanning over conventional x-ray radiographs. Using this new technology, we examined the subcellular changes associated with hypoxic stress to cultured adult rabbit cardiac myocytes. To simulate the ATP depletion and reductive stress of anoxia, we exposed myocytes to 2.5 mM NaCN, a potent inhibitor of aerobic mitochondrial metabolism. We also inhibited glycolysis with 2-deoxyglucose, because glycolysis does not sustain ATP levels during myocardial ischemia/anoxia because of rapid exhaustion of glycolytic substrates.

Basic aspects of cell structure include size, shape, and surface topography. Confocal microscopy combined with three-dimensional reconstruction techniques provided this structural information for single living myocytes. Myocytes were loaded with calcein, a fluorophore whose fluorescence is not affected by physiological changes of pH and ion concentrations (Haugland, 1992). Confocal images were then collected as the plane of focus was advanced in 1.2-μm increments through the entire thickness of the cell. The data sets were reconstructed to represent myocytes as solid objects using contour-dependent shading to enhance the perception of surface topography. These volume renderings of living cells rivaled scanning electron micrographs of fixed myocytes in clarity and detail (compare Figs. 2 and 3). Using this technique during chemical hypoxia, we observed extensive cell surface blebbing and a 30% decrease of cell volume coincident with the onset of hypercontracture (Figs. 3 and 4), as observed previously by scanning electron microscopy in models of hypoxic injury to cardiac myocytes (Schwartz et al., 1984). These events precede loss of sarcolemmal integrity and the onset of cell death.

Mitochondrial permeability transition after hypercontraction and mitochondrial Ca^{2+} loading

Several different parameter-sensitive fluorophores were used in this study. By exploiting spectral differences between individual probes, two probes could be imaged simultaneously. A multi-line argon-krypton laser provided excitation at 488 and 568 nm and dichroic and barrier filters separated emitted fluorescence by wavelength to different photomultipliers. Dual-labeling with TMRM and Fluo-3 allowed us to monitor free Ca^{2+} and mitochondrial $\Delta\Psi$ simultaneously. During chemical hypoxia, cytosolic Ca^{2+} increased and apparently caused cell shortening and hypercontraction (Fig. 7).

Unexpectedly, mitochondria remained polarized until after the onset of hypercontraction and bleb formation (Figs. 5 and 7). At the onset of hypercontraction, mitochondria loaded heavily with Ca^{2+} and depolarized abruptly shortly afterwards (Fig. 7). Depolarization was followed by release of Ca^{2+} from mitochondria. This sequence of mitochondrial Ca^{2+} loading, depolarization and Ca^{2+} release resembles the so-called mitochondrial membrane permeability transition described in isolated mitochondria (Hunter et al., 1976; Gunter and Pfeiffer, 1990; Szabo and Zoratti, 1991; Fournier et al., 1987; Crompton et al., 1988). Ca^{2+} uptake into the matrix induces the opening of a very high conductance "megachannel" (Szabo and Zoratti, 1991). Megachannel opening causes membrane depolarization and subsequent release of mitochondrial Ca^{2+} and other solutes. Cyclosporin A, an immunosuppressant cyclic peptide, blocks the mitochondrial megachannel (Szabo and Zoratti, 1991; Fournier et al., 1987; Crompton et al., 1988). Nazareth and co-workers (1991) recently reported that cyclosporin A delays anoxic killing to myocytes. In preliminary experiments, we also found that cyclosporin A in combination with butanedione monoxime prevented hypercontraction, mitochondrial depolarization, and cell death in a model of reperfusion injury to adult rabbit cardiac myocytes (Chacon et al., 1993b). Taken together, these findings indicate that a membrane permeability transition is most likely occurring after hypercontraction and mitochondrial Ca^{2+} loading during chemical hypoxia. Moreover, a permeability transition may be one of the mechanisms actually contributing to cell killing.

Mitochondrial protonmotive force estimated by laser scanning confocal microscopy

The high energy state that drives ATP synthesis, ion transport, and most other energy-requiring reactions in mitochondria is the electrochemical difference of protons across the inner mitochondrial membrane ($\Delta\mu_{H^+}$) or, equivalently, the protonmotive force (Δp). Δp is comprised of two components: $\Delta\Psi$ and ΔpH, as described by Eq. 1. Here, using laser

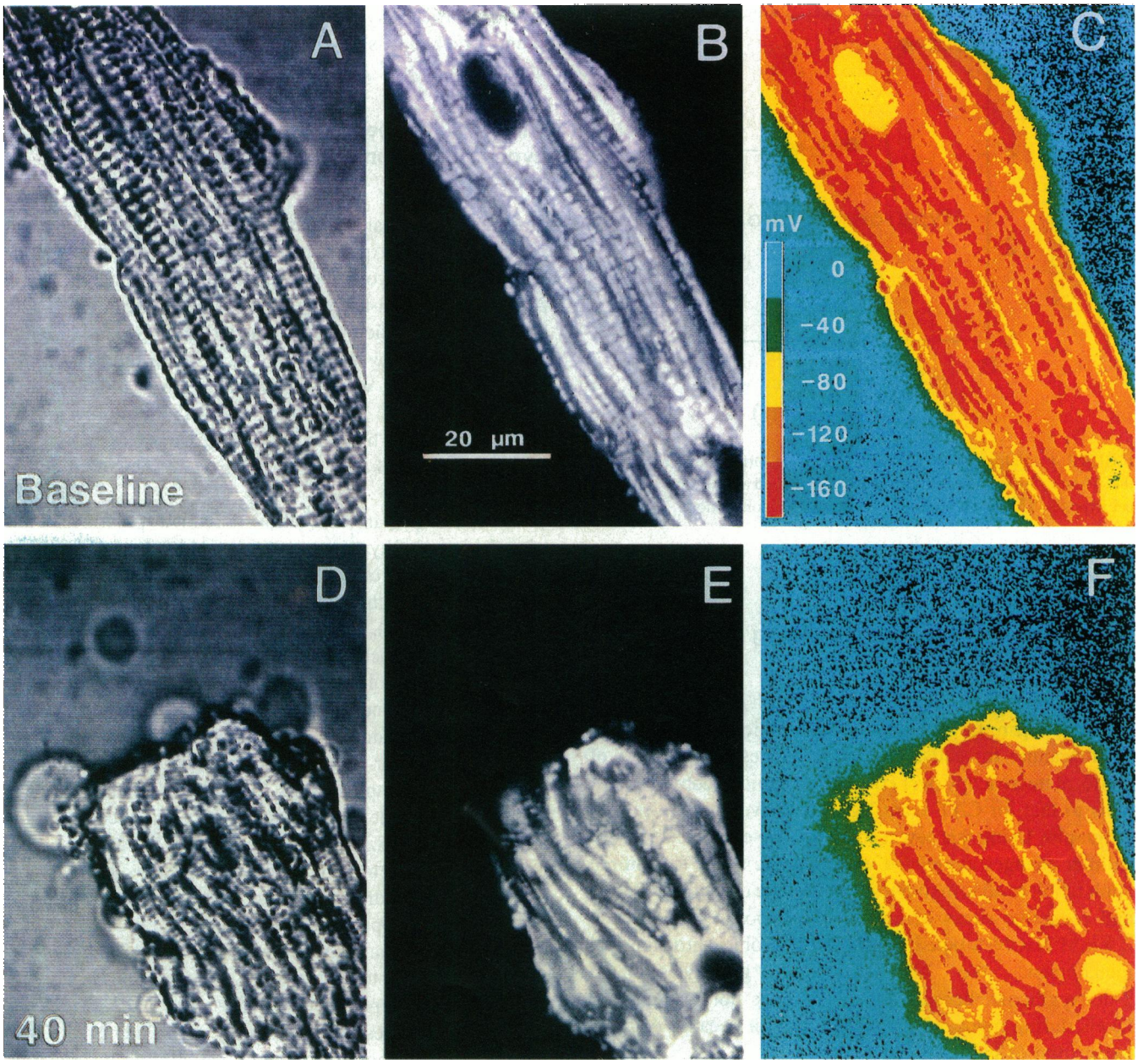

FIGURE 5 Intracellular distribution of electrical potential in a cultured cardiac myocyte during chemical hypoxia: *A* 1-day cultured cardiac myocyte was loaded with TMRM and incubated in KRH with 150 nM TMRM as described in Materials and Methods. The myocyte was imaged before (*A–C*) and after 40 min of chemical hypoxia (*D–F*). *A* and *D* are nonconfocal bright field images collected with a transmitted light detector. *B* and *E* are unprocessed confocal fluorescence images obtained simultaneously using 568 nm excitation light and an enhance circuit setting of +4. *C* and *F* are the respective pseudocolored images of *B* and *E* showing the intracellular distribution of electrical potential. Electrical potential was calculated by application of the Nernst equation as described in Materials and Methods. Colors represent different potentials: blue, 20 to −20 mV; green, −20.1 to −60 mV; yellow, −60.1 to −100 mV; orange, −100.1 to −140 mV; and red, −140.1 to −180 mV. Areas of most negative intracellular electrical potential (orange and red) represent mitochondria.

scanning confocal microscopy, we measured $\Delta\Psi$ of individual mitochondria inside single cells from the equilibrium distribution of TMRM by extension of the approach of Farkas et al. (1989). In addition, we measured ΔpH by ratio imaging of SNARF-1, a pH-sensitive fluorophore (Fig. 1) (Bassnett et al., 1990; Sesek et al., 1991).

Ideally, cationic fluorophores like TMRM or rhodamine 123 distribute into negatively charged compartments in accordance with the Nernst equation (Eq. 5). However, some cationic fluorophores, including rhodamine 123, quench when taken up into mitochondria, and show nonspecific binding independent of the electrical potential (Emaus et al., 1986; Bunting et al., 1989). Correction factors may be applied to correct for these effects, but each correction introduces a new degree of uncertainty. Newer fluorophores, such as TMRM, seem to lack these undesirable qualities and may be more suited for monitoring mitochondrial membrane potential (Farkas et al., 1989; Ehrenberg et al., 1988).

At equilibrium, a 10:1 accumulation ratio for a permeant cation corresponds to a −60 mV potential, a 100:1 ratio to

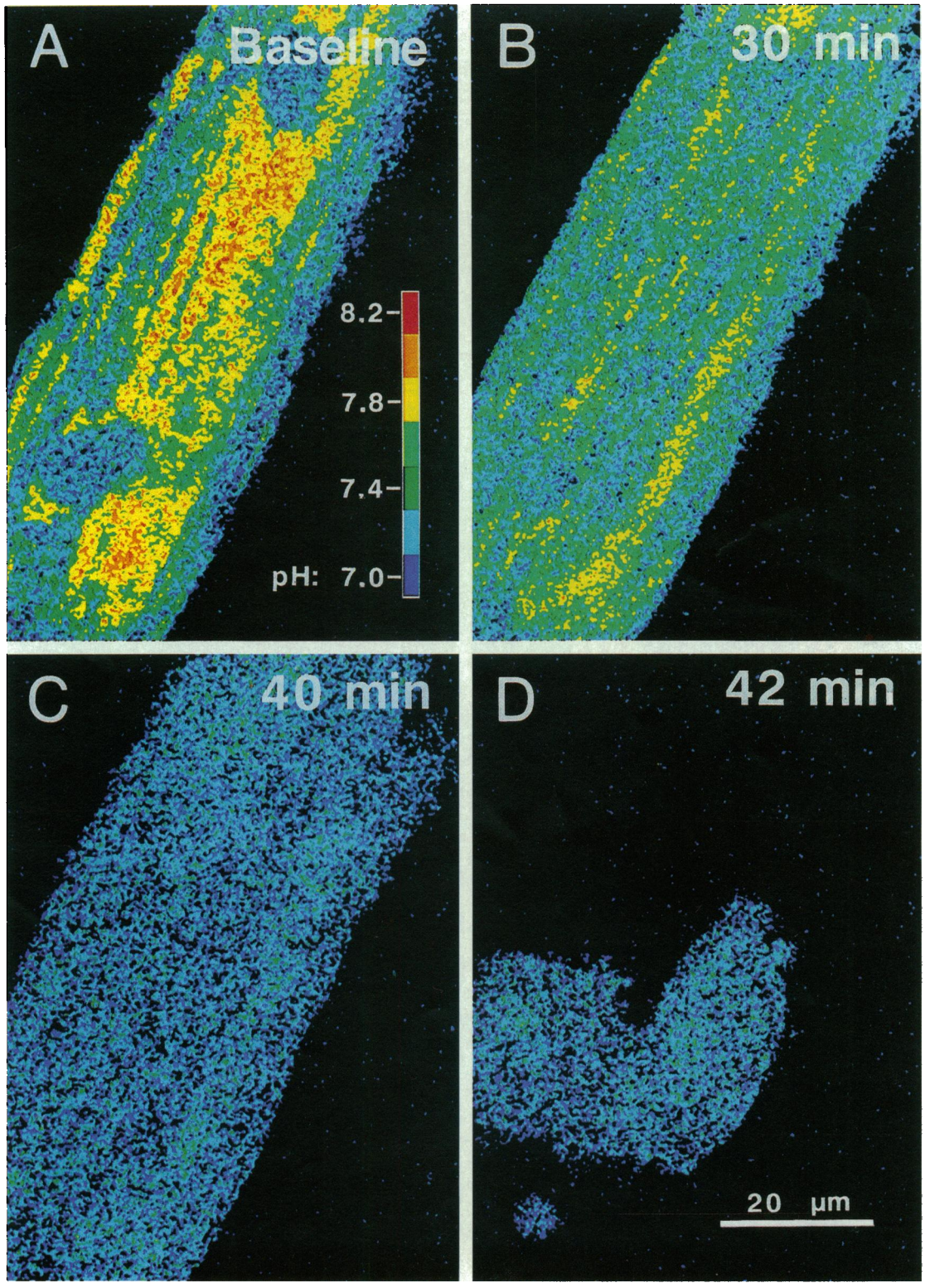

FIGURE 6 Intracellular distribution of pH in a cardiac myocyte during chemical hypoxia: a 1-day cultured cardiac myocyte was loaded with SNARF-1, and intracellular pH was measured by confocal ratio imaging as described in Materials and Methods before (*A*) and after 30 min (*B*), 40 min (*C*), and 42 min (*D*) of chemical hypoxia.

a −120 mV potential, a 1000:1 ratio to a −180 mV potential, and so forth. For excitable cells like cardiac myocytes, a plasma membrane potential of −90 mV and a mitochondrial membrane potential of up to −150 mV are typical expected values. As the electrical potentials are additive with respect to the extracellular space, mitochondria inside an excitable cell may be as much as −240 mV more negative that the extracellular space, corresponding to a 10,000:1 accumulation ratio. Such high fluorophore gradients are impossible to measure using typical 8-bit frame memories storing only

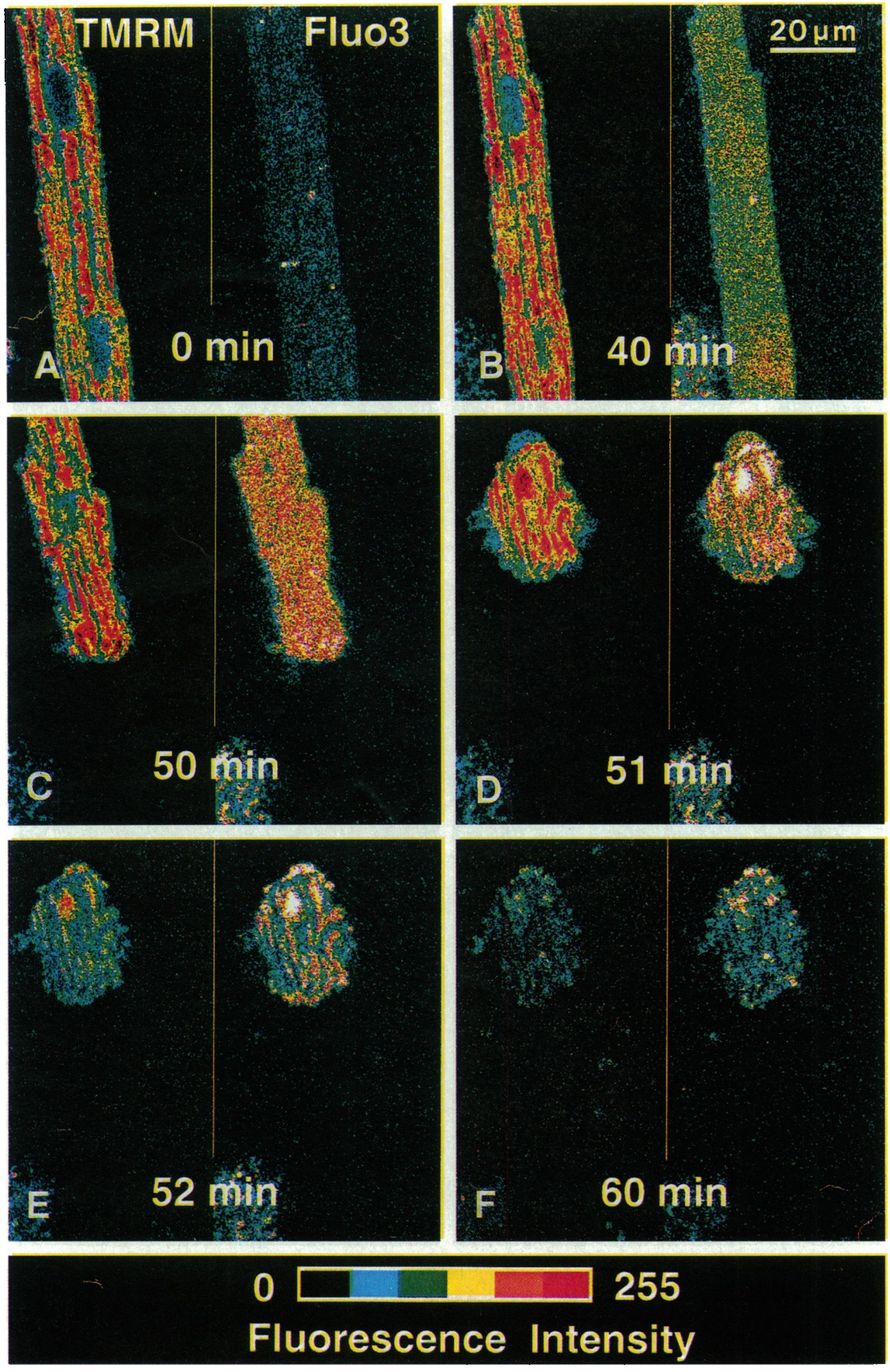

FIGURE 7 Intracellular free calcium and mitochondrial membrane $\Delta\Psi$ in a cardiac myocyte during chemical hypoxia: a 1-day cultured cardiac myocyte was co-loaded with TMRM and Fluo-3, and red and green confocal fluorescence images were acquired as described in Materials and Methods before (*A*) and after 40 min (*B*), 50 min (*C*), 51 min (*D*), 52 min (*E*) and 60 min (*F*) of chemical hypoxia. Each panel shows the red fluorescence of TMRM on the left and the green fluorescence of Fluo-3 on the right. The images are pseudocolored using a linear scale of fluorescence intensity.

256 gray levels of light intensity. To expand our dynamic range of measurement, we employed an enhance circuit (analogous to gamma circuits, long used in scanning electron microscopy) to apply a logarithmic function to the output of the photomultiplier, effectively condensing high-end signals into the available 256 pixel levels of video memory (Table 1).

Using extracellular fluorescence as the baseline intensity, pseudocolor look-up tables were generated to show the distribution of electrical potential inside single myocytes. Subsarcolemmal, intermitochondrial and nuclear regions had a uniform voltage of about −80 mV relative to the outside, very close to the expected sarcolemmal $\Delta\Psi$ of cardiac myocytes (Fig. 5). Electrical potential of mitochondria was in the range of −140 to −180 mV relative to the extracellular space. Mitochondrial $\Delta\Psi$ is the difference between mitochondrial and cytosolic electrical potential. Thus, mitochondrial $\Delta\Psi$ estimated in this way ranged between −60 and −100 mV.

Because of the diameter of mitochondria (1 μm) in relation to the thickness of the confocal slice (0.8–0.9 μm with the equipment used, Lemasters et al., 1993), most mitochondria did not extend all the way through the thickness of the confocal slice. Thus, the apparent mitochondrial volume fraction in the two-dimensional images seems larger than it really is. As a result for many mitochondrial profiles, TMRM accumulation from confocal images represents a weighted average of mitochondrial and cytosolic fluorescence and an underestimate of true matrix TMRM concentration. Thus, the highest apparent uptake ratios measured in the confocal images represent mitochondria centered within the confocal section. $\Delta\Psi$ from these highest uptake ratios are most likely closest to true mitochondrial $\Delta\Psi$.

Intracellular pH in cytosol and mitochondria was measured using SNARF-1. SNARF-1 was loaded using its membrane-permeant acetoxymethyl ester derivative. Inside cells, SNARF-1 free acid was liberated by endogenous esterases. Like other AM-loaded fluorophores in cardiac myocytes, SNARF-1 accumulated into both cytosol and mitochondria (Gunter et al., 1988; Lemasters et al., 1990; Chacon et al., 1992a). We exploited this phenomenon to image mitochondrial and cytosolic pH simultaneously using confocal microscopy. Subsarcolemmal and nuclear areas had a pH averaging about 7.1, but in regions corresponding to mitochondria, pH was as high as 8.0 (Fig. 6). Thus, maximum ΔpH across the mitochondrial membrane was 0.9 units. From these measurements of maximum $\Delta\Psi$ and ΔpH, we can estimate using Eq. 2 a mitochondrial Δp of about −155 mV in resting adult cardiac myocytes. These values for $\Delta\Psi$, ΔpH and Δp agree generally with previous values determined in large cell populations by independent techniques (Hoek et al., 1980; Rottenberg, 1975).

Early decline of mitochondrial ΔpH during chemical hypoxia

During chemical hypoxia, ΔpH gradually declined (Fig. 6). After 40 min of chemical hypoxia, ΔpH collapsed entirely, although mitochondrial $\Delta\Psi$ was virtually unchanged. The basis for the selective decrease of ΔpH is unclear. Cardiac myocytes contain high concentrations of the high energy phosphate compounds, ATP, and creatine phosphate. Hydrolysis of these compounds during hypoxic stress causes an eightfold increase of Pi inside the cells (Steenbergen et al., 1992). Pi is a weak acid that collapses ΔpH in mitochondria in vitro (see Emaus et al., 1986). Thus, the accumulation of intracellular Pi during chemical hypoxia may account for the early collapse of ΔpH in our experiments.

CONCLUSION

Our findings illustrate the main advantages of laser scanning confocal microscopy for studying living cells: 1) thin optical sectioning of thick cells, 2) resolution in three dimensions from multiple optical slices, and 3) subcellular resolution of parameter-sensitive fluorescent probes. With laser scanning confocal microscopy, we uncovered a unique sequence of subcellular events as chemical hypoxia progressed in cultured adult rabbit cardiac myocytes. After inhibition of cellular ATP synthesis with cyanide and 2-deoxyglucose, mitochondrial ΔpH gradually collapsed. Subsequently, cytosolic and mitochondrial Ca^{2+} began to increase. As Ca^{2+} increased, myocytes began to shorten, and then to hypercontract and bleb. In rapid succession, hypercontraction led to mitochondrial Ca^{2+} loading, depolarization and, finally, release of Ca^{2+} from mitochondria. These events were followed ultimately by breakdown of the plasma membrane permeability barrier and cell death. Our future studies will pursue the mechanisms underlying these new phenomena in models of hypoxic, ischemic, and reperfusion injury to cardiac myocytes.

We thank Mr. Yukio Tanaka and Mr. C. Wesley Lane for expert assistance in electron microscopy.

REFERENCES

Bassnett, S., L. Reinisch, and D. C. Beebe. 1990. Intracellular pH measurement using single excitation-dual emission fluorescence ratios. *Am. J. Physiol.* 258:C171–C178.

Bond, J. M., B. Herman, and J. J. Lemasters. 1991. Recovery of cultured rat neonatal myocytes from hypercontracture after chemical hypoxia. *Res. Commun. Chem. Pathol. Pharmacol.* 71:195–208.

Bunting, J. R., T. V. Phan, E. Kamali, and R. M. Dowben. 1989. Fluorescent cationic probes of mitochondria. *Biophys. J.* 56:979–993.

Chacon, E., R. Ulrich, and D. Acosta. 1992a. A digitized fluorescence-imaging study of mitochondrial Ca^{2+} increase by doxorubicin in cardiac myocytes. *Biochem. J.* 281:871–878.

Chacon, E., G. Zahrebelski, J. M. Reece, A.-L. Nieminen, B. Herman, and J. J. Lemasters. 1992b. Protonmotive force measurements in single cells by laser scanning confocal microscopy: collapse of ΔpH precedes collapse of $\Delta\Psi$ and hypercontracture in rabbit cardiac myocytes during chemical hypoxia. *Toxicol. Lett. (Suppl.).* 221s–222s.

Chacon, E., D. Acosta, J. M. Bond, A.-L. Nieminen, and J. J. Lemasters. 1993a. Procedures for assessment of in vitro cardiotoxicitity. *In* Handbook of Toxicology In Vitro. C. M. Nadolney, editor. CRC Press, Boca Raton, FL. In press.

Chacon, E., I. S. Harper, J. M. Reece, B. Herman, and J. J. Lemasters. 1993b. Rescue of adult rabbit cardiac myocytes from ischemia/reperfusion injury

by cyclosporin A and butanedione monoxime. *FASEB J.* 7:94*a*. (Abstr.)

Crompton, M., H. Ellinger, and A. Costi. 1988. Inhibition by cyclosporin A of a Ca^{2+}-dependent pore in heart mitochondria activated by inorganic phosphate and oxidative stress. *Biochem. J.* 255:357–360.

Ehrenberg, B. V., V. Montana, M.-D. Wei, J. P. Wuskell, and L. M. Loew. 1988. Membrane potential can be determined in individual cells from the Nernstian distribution of cationic dyes. *Biophys. J.* 53:785–794.

Emaus, R. K., R. Grunwald, and J. J. Lemasters. 1986. Rhodamine 123 as a probe of transmembrane potential in isolated rat-liver mitochondria: spectral and metabolic properties. *Biochim. Biophys. Acta.* 850:436–448.

Farkas, D. L., M.-D. Wei, P. Fabbroriello, J. H. Carson, and L. M. Loew. 1989. Simultaneous imaging of cell and mitochondrial membrane potentials. *Biophys. J.* 56:1053–1068.

Fournier, N., G. Ducet, and A. Crevat. 1987. Action of cyclosporine on mitochondrial calcium fluxes. *J. Bioenerg. Biomembr.* 19:297–303.

Gores, G. J., A.-L. Nieminen, K. E. Fleishman, T. L. Dawson, B. Herman, and J. J. Lemasters. 1988. Extracellular acidosis delays onset of cell death in ATP-depleted hepatocytes. *Am. J. Physiol.* 255:C315–C322.

Gunter, T. E., D. Restroepo, and K. K. Gunter. 1988. Conversion of esterified Fura-2 and Indo-1 to Ca^{2+} sensitive forms by mitochondria. *Am. J. Physiol.* 255:C304–C310.

Gunter, T. E., and Pfeiffer, D. R. 1990. Mechanisms by which mitochondria transport calcium. *Am. J. Physiol.* 258:C755-C786.

Haddad, J., M. L. Decker, L.-C. Hsieh, M. Lesch, A. M. Samarel, and R. S. Decker. 1988. Attachment and maintenance of adult rabbit cardiac myocytes in primary culture. *Am. J. Physiol.* 255:C19–C27.

Haugland, R. P. 1992. Handbook of Fluorescent Probes and Research Chemicals. Molecular Probes, Inc., Eugene, OR.

Hoek, J. B., D. G. Nicholls, and J. R. Williamson. 1980. Determination of the mitochondrial protonmotive force in isolated hepatocytes. *J. Biol. Chem.* 255:1458–1464.

Hunter, D. R., R. A. Haworth, and J. H. Southard. 1976. Relationship between configuration, function, and permeability in calcium-treated mitochondria. *J. Biol. Chem.* 251:5069–5077.

Kawanishi, T., A.-L. Nieminen, B. Herman, and J. J. Lemasters. 1991. Suppression of Ca^{2+} oscillations in cultured rat hepatocytes by chemical hypoxia. *J. Biol. Chem.* 266:20062–20069.

Lemasters, J. J., C. J. Stemkowski, S. Ji, and R. G. Thurman. 1983. Cell surface changes and enzyme release during hypoxia and reoxygenation in the isolated, perfused rat liver. *J. Cell Biol.* 97:778–786.

Lemasters, J. J., A.-L. Nieminen, G. J. Gores, T. L. Dawson, B. E. Wray, T. Kawanishi, K. Florine-Casteel, J. M. Bond, and B. Herman. 1990. Multiparameter digitized video microscopy (MDVM) of hypoxic cell injury. *In* Optical Microscopy for Biology. B. Herman and K. A. Jacobson, editors. Alan R. Liss, Inc., New York. 523–542.

Lemasters, J. J., E. Chacon, G. Zahrebelski, J. M. Reece, and A.-L. Nieminen. 1993. Laser scanning confocal microscopy of living cells. *In* Optical Microscopy: Emerging Methods and Applications. B. Herman and J. J. Lemasters, editors. Academic Press, San Diego, CA. 339–354.

Minta, A., J. Kao, and R. Tsien. 1989. Fluorescent indicators for cytosolic calcium based on rhodamine and fluorescein chromophores. *J. Biol. Chem.* 264:8171–8178.

Mitchell, P. 1966. Chemiosmotic coupling in oxidative and photosynthetic phosphorylation. *Biol. Rev.* 41:445–502.

Nazareth, W., N. Yafei, and M. Crompton. 1991. Inhibition of anoxia-induced injury in heart myocytes by cyclosporin A. *J. Mol. Cell. Cardiol.* 23:1351–1354.

Nicholls, D. G. 1974. The influence of respiration and ATP hydrolysis on the proton-electrochemical gradient across the inner membrane of rat-liver mitochondria as determined by ion distribution. *Eur. J. Biochem.* 50:305–315.

Rottenberg, H. 1975. Measurements of transmembrane electrochemical proton gradients. *J. Bioenerg.* 7:63–76.

Schwartz, P., H. M. Piper, M. A. Spahr, and P. G. Spieckemann. 1984. Ultrastructure of cultured adult myocardial cells during anoxia and reoxygenation. *Am. J. Pathol.* 115:349–361.

Sesek, O., N. Henry-Tolume, F. Sureau, and J. Bolard. 1991. SNARF-1 as an intracellular pH indicator in laser microspectrofluorometry: A critical assessment. *Anal. Biochem.* 193:49–54.

Steenbergen, C., M. E. Pearlman, R. E. London, and E. Murphy. 1992. Mechanisms of preconditioning. *Circ. Res.* 72:112–125.

Szabo, I., and M. Zoratti. 1991. The giant channel of the inner mitochondrial membrane is inhibited by cyclosporin A. *J. Biol. Chem.* 266:3376–3379.